

Superconductivity-enhanced spin pumping: Role of Andreev resonances

Mostafa Tanhayi Ahari and Yaroslav Tserkovnyak

Department of Physics and Astronomy, University of California, Los Angeles, California 90095, USA

We describe a simple hybrid superconductor|ferromagnetic-insulator structure manifesting spin-resolved Andreev bound states in which dynamic magnetization is employed to probe spin related physics. We show that, at low bias and below T_c , the transfer of spin angular momentum pumped by an externally driven ferromagnetic insulator is greatly affected by the formation of spin-resolved Andreev bound states. Our results indicate that these bound states capture the essential physics of condensate-facilitated spin flow. For finite thicknesses of the superconducting layer, comparable to the coherence length, resonant Andreev bound states render highly transmitting subgap spin transport channels. We point out that the resonant enhancement of the subgap transport channels establishes a prototype Fabry-Pérot resonator for spin pumping.

Introduction.—Spatial variations in the superconducting order in a finite region lead to the formation of spin-degenerate Andreev bound states (ABSs) with discrete excitation energies below the superconducting gap [1]. An externally applied magnetic field or proximity to a ferromagnetic order, on the other hand, can induce spin splitting in the ABSs that results into spin-resolved ABSs [2]. In this paper, we consider a normal metal (N) sandwiched between a superconductor (S) and a ferromagnetic insulator (FI) that serves as a simple platform with spin-resolved ABSs, which are localized in the N layer. The nonequilibrium pure spin current engendered from the externally driven FI—spin pumping—is utilized to probe spin transport in an S|N|FI hybrid structure. The spin pumping generated from a time-dependent magnetization, on the other hand, is a flow of spin angular momentum into adjacent materials that dissipates energy of the ferromagnet [3]. We suggest that the magnetic damping increase in superconducting hybrid multilayers Nb|Ni₈₀Fe₂₀ and NbN|GdN reported, respectively, in Refs. [4] and [5] may be attributed to the resonant enhancement of the spin pumping discussed here.

In the context of superconducting spintronics, combining an *s*-wave superconducting order, favoring electrons to form a singlet state, with a ferromagnetic order, favoring spin alignment, leads to a powerful enhancement or reduction of angular momentum transfer [6, 7]. The angular momentum transfer, as a central effect in spintronics, is greatly modified on account of two major underlying causes: the itinerant spin-polarized quasiparticles (QPs) with long spin-coherence lengths [8, 9] and the creation of spin-triplet Cooper pairs [10–12] induced at highly spin-active regions or complex magnetic multilayers [13]. Here, the spin pumping in an S|N|FI hybrid structure, however, is an interplay between spin-polarized QPs and spin-triplet Cooper pairs, which are dynamically generated by the excited FI [14, 15]. The subgap ABSs accommodate the spin-polarized QPs and spin-triplet Cooper pairs that for a sufficiently thin S layer can tunnel across and contribute to the spin current. To collect the spin current we have placed a spin reservoir N_r , comprising an N_r |S|N|FI structure (see Fig. 1).

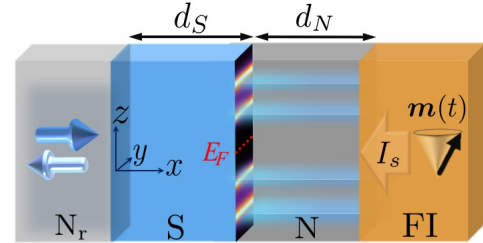


FIG. 1. Schematic sketch for an N_r |S|N|FI hybrid structure. The FI region with precessing magnetization $\mathbf{m}(t)$ injects spin angular momentum, I_s , that is carried by the QPs into the reservoir N_r (spin pumping). For finite thicknesses of the S and N layers ($d_S, d_N \sim$ coherence length) the resonant ABSs provide highly transmitting transport channels for spin pumping. Here, for example, we show four resonant channels with two positive-energy ABSs. The energies are measured with respect to the Fermi energy E_F depicted in the middle.

While spin pumping has been considered as a new probe of spin dynamics in a superconducting thin film [16] and tunable pure spin supercurrents [17], here we propose to study spin-resolved Andreev resonances by means of spin pumping.

Spin-resolved ABS.—We will determine the subgap spin-resolved ABSs by studying the resonant conditions for the spin transport in an N_r |S|N|FI hybrid structure. In order to establish the pumped spin current in the presence of superconducting and dynamic ferromagnetic orders, we solve a time-dependent scattering problem [15, 18], which accounts for the relevant processes such as Andreev reflection (AR), ABS, and a dynamic triplet-pairing generation. For subgap energies, the full scattering matrix develops peak structures marking resonant bound states [19] (ABSs), which result in highly transmitting subgap transport channels for the spin flow. While we identify the Andreev resonances in the ballistic regime, we do not expect their perturbation by a weak disorder to significantly modify the spectroscopic aspects of spin pumping (which should be governed by the underlying dynamic mixing between the superconducting

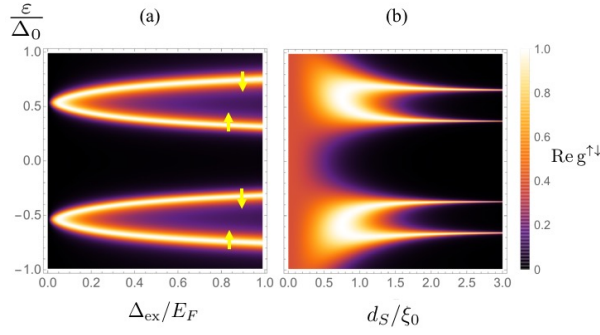


FIG. 2. Profile of $\text{Re } g^{\uparrow\downarrow}$ for $d_N/\xi_0 = 1$. (a) Assuming fixed S layer thickness ($d_S/\xi_0 = 1.5$), the spectral overlap of the spin-split Andreev levels can be modified by Δ_{ex} . (b) At the finite thicknesses of the S, $d_S \gtrsim \xi_0$, the Andreev resonances establish highly transmitting transport channels. Here, we have set $\Delta_{\text{ex}}/E_F = 0.4$.

singlet and triplet components). To capture the essential effect of interfacial scattering on the spin-pumping enhancement, we will consider an interface disorder at $x = d_S$.

We proceed with establishing notations and key features of the scattering. The incident QPs from the reservoir onto the $N_r|S$ interface can either transmit across the S or reflect as holes back into the reservoir, a process known as AR. The AR amplitude for an incident QP with energy ε is given by

$$r_A^\infty = \begin{cases} e^{-i \arccos(\varepsilon/\Delta)}, & |\varepsilon| < \Delta, \\ \frac{\varepsilon - \varepsilon \sqrt{1 - \Delta^2/\varepsilon^2}}{\Delta}, & |\varepsilon| > \Delta, \end{cases} \quad (1)$$

where Δ is the superconducting pair-potential [2]. The AR amplitude given in Eq. (1), by focusing on the interface, assumes a bulk S (a thick S layer) [15]. A nonzero probability of QP transmission for the thin S as well as an interfacial disorder can reduce the AR probability, which we address below. The transmitted QPs with spin $\sigma \in \{\uparrow, \downarrow\}$ propagate through the normal metal junction and acquire a spin-dependent phase $e^{i\vartheta_\sigma}$ upon reflection from the FI interface, where the FI region is considered an exchange-splitting insulator for the QPs [21]. This renders the full scattering matrix to be merely a reflection matrix, which is block diagonal in the spin space due to the conservation of the QP spin during each individual scattering event. Consequently, multiple ARs at the $N|S$ along with spin-dependent reflections at the $N|FI$ interfaces constitute the full scattering matrix.

The spin-active interface $N|FI$, upon reflection, rotates a noncollinear QP spin around the FI magnetization axis, which in turn for a driven magnetization leads to generation of a nonequilibrium spin current detected in N_r [22]. The conductance determining the transport of this spin current, known as the mixing conductance $g^{\uparrow\downarrow}$, is given

by

$$g^{\uparrow\downarrow} = \sum_{n,m} (\delta_{m,n} - r_{ee,mn}^\uparrow r_{ee,mn}^{\downarrow*} + r_{he,mn}^\uparrow r_{he,mn}^{\downarrow*}), \quad (2)$$

where r_{ee}^σ and r_{he}^σ represent the total spin- σ electron-to-electron and electron-to-hole reflection matrices in the $S|N|FI$ hybrid structure, respectively [14, 18]. The indices n and m refer to transport channels the number of which can be determined by transverse thickness of the normal metal layer [2]. The reflection matrices in Eq. (2) are written in the basis where the spin quantization axis is parallel to the magnetization in the FI (the exact expressions for the reflection amplitudes in the ballistic regime can be found in the Supplemental Material [15]). In the following, we provide the results for the single-channel scattering and postpone discussing the case of multichannel scattering to the Supplemental Material [15].

Generically, the mixing conductance given in Eq. (2) is a complex number the real part of which governs the average spin pumping and the associated Gilbert damping [18]. After a straightforward calculation in the ballistic regime, three distinct regimes are recognized for subgap energies:

$$\text{Re } g^{\uparrow\downarrow} \approx \begin{cases} 1 - \cos \vartheta & d_S \ll \xi_0 \\ \gamma^2/(\gamma^2 + \beta^2) & d_S \sim \xi_0 \\ 0 & d_S \gg \xi_0 \end{cases}, \quad (3)$$

where $\gamma = \exp[-2\sqrt{1 - \varepsilon^2/\Delta_0^2} d_S/\xi_0]$, $\beta = [\cos(4d_N\varepsilon/\xi_0\Delta_0 + 2\theta_A) - \cos\vartheta]/4\sin\vartheta\sin^2\theta_A$, and $\theta_A \equiv -\arccos(\varepsilon/\Delta_0)$. The mixing angle defined as $\vartheta \equiv \vartheta_\uparrow - \vartheta_\downarrow$ is controlled by the FI exchange interaction Δ_{ex} [15]. Here, Δ_0 and ξ_0 are the superconducting gap and coherence length at zero temperature, respectively. Evidently, $\text{Re } g^{\uparrow\downarrow}$ displays a resonant behavior associated with the intermediate S thickness. The resonant energy levels correspond to the ABS energies ε_A determined by ($\beta = 0$):

$$\varepsilon_A = \Delta_0 \text{sign} \left[\sin \left(\frac{2d_N\varepsilon_A}{\xi_0\Delta_0} \pm \frac{\vartheta}{2} \right) \right] \cos \left(\frac{2d_N\varepsilon_A}{\xi_0\Delta_0} \pm \frac{\vartheta}{2} \right). \quad (4)$$

When the exchange interaction is absent, that is, $\vartheta = 0$, Eq. (4) yields a pair of solutions $(-\varepsilon_A, \varepsilon_A)$, which is a consequence of the particle-hole symmetry imposed on the scattering formalism [15]. A nonzero mixing angle ϑ , on the other hand, by lifting the spin degeneracy of each level results in the spin-resolved ABSs with the following energies $(-\varepsilon_A^\pm, \varepsilon_A^\pm)$. As an outcome, the spectral overlap of the spin-split bound states can be controlled by the exchange interaction of the FI [e.g., see Fig. 2(a)]. We emphasize that, following Eq. (3), only at $d_S \sim \xi_0$ the resonant ABSs establish highly transmitting transport channels for the spin flow, which is greatly enhanced

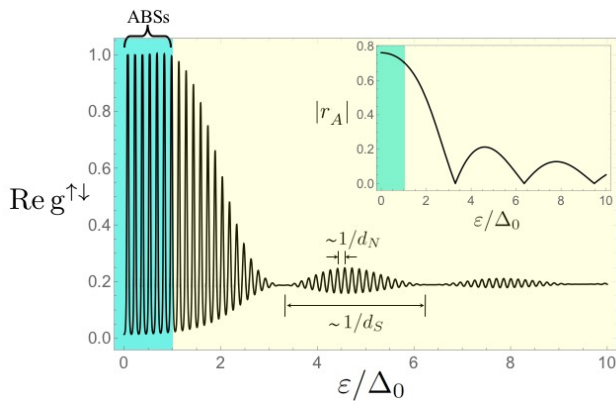


FIG. 3. Geometric resonances of $\text{Re } g^{\uparrow\downarrow}$. The Fabry-Pérot oscillations happen when the corresponding AR probability $|r_A|$ is nonzero (the inset plot shows the probability of AR vs energy). For a fixed Δ_{ex} , the Fabry-Pérot oscillations are determined by d_N that for $\varepsilon > \Delta_0$ get modulated with a frequency determined by d_S (i.e., energies for which $|r_A| = 0$). Here, we have adopted the following parameters: $d_S/\xi_0 = 1$, $d_N/\xi_0 = 10$, and $\Delta_{\text{ex}}/E_F = 0.2$.

compared to either a bulk or no S layer [see Fig. 2(b)]. This is one of the main results of this paper.

In the limit where $d_N \rightarrow 0$, Eq. (4) can be reduced to the well known result [23] for ABSs with magnetically active interfaces, $\varepsilon_A/\Delta_0 = \pm \cos \vartheta/2$. We highlight the fact that Eq. (4) is a condition for a constructive quantum interference in a Rowell-McMillan process for the QPs [12], that is, four times crossing N with two Andreev conversions as well as two reflections from FI, once as electron and once as hole. It is clear that a constructive interference for QPs inside the normal layer remains intact as long as the probability of the AR is nonzero. This captures the essential physics of a two-mirror Fabry-Pérot resonator with a resonator length $2d_N$, which we shall describe now. The N|FI and S|N interfaces operate as “mirrors” for the QPs that give rise, respectively, to a spin-dependent specular reflection (a spin-dependent mirror) and a phase-conjugating mirror, which retroreflects electrons with energy $E_F + \varepsilon_A$ as holes with energy $E_F - \varepsilon_A$ [24]. The resonant enhancement of a Fabry-Pérot device occurs when its mirrors have a near unity reflection probability [25]. Here, the N|FI interface reflects all the incident QPs with probability 1, while the retroreflection probability of the S|N interface, on the other hand, is determined by the AR probability. Therefore, the Fabry-Pérot enhancement is in accordance with the AR amplitude, which for an S with a thickness d_S [15] is given by

$$r_A = \frac{(1 - \gamma)r_A^\infty}{1 - \gamma(r_A^\infty)^2}. \quad (5)$$

For subgap energies, in the limiting case of $d_S > \xi_0$, we get $\gamma \ll 1$ or equivalently $|r_A| \approx 1$, for which the resonant

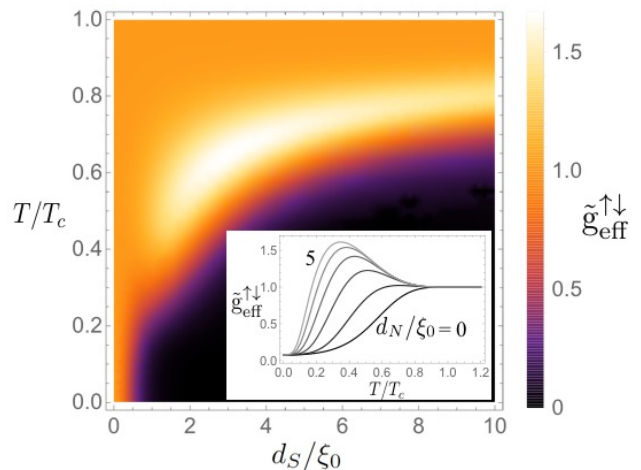


FIG. 4. The normalized effective conductance, $\tilde{g}_{\text{eff}}^{\uparrow\downarrow}$, for subgap temperatures and intermediate thickness $d_S \sim \xi_0$ showing a significant enhancement relative to the normal case near T_c . As the S gap shrinks, with the increase of temperature, the enhancement peak location creeps up to higher d_S , which ultimately diminishes for higher temperatures near T_c . Here, we have set $d_N/\xi_0 = 2.5$. The inset shows that the enhancement feature happens for all $0 \leq d_N/\xi_0 \leq 5$ when $d_S/\xi_0 = 1$. For the above plots, we have used $\Delta_{\text{ex}}/E_F = 0.2$.

enhancement of a Fabry-Pérot device is expected. For energies above the gap, on the other hand, the AR reflection amplitude decreases. This results in highly transmissive channels near $\varepsilon \gtrsim \Delta_0$, which rapidly decline for higher energies (see Fig. 3).

In addition to the QP interference in the normal layer (Rowell-McMillan resonance), which leads to the mixing conductance oscillation, above the gap a quantum interference inside the S layer can take place. An incident electronlike QP interferes with a holelike QP reflected from the other S|N interface, which may result in $|r_A| = 0$. The process known as Tomasch oscillations [26] occurs for QP energies $\varepsilon_n/\Delta_0 = \sqrt{1 + (n\pi\xi_0/2d_S)^2}$ with integer n , which modulates the amplitude for the Fabry-Pérot oscillations. The Rowell-McMillan and Tomasch based geometric resonances of $\text{Re } g^{\uparrow\downarrow}$ are shown in Fig. 3.

Spin pumping enhancement.—The spin pumping is generated by the variations in the magnetization direction $\mathbf{m}(t)$ [3, 10, 27]. For sufficiently slow variations, to the first order in the pumping parameter frequency $|\partial_t \mathbf{m}|$, the spin pumping can be written in terms of the instantaneous mixing conductance in the magnetization coordinate system, that is, Eq. (2). Consequently, the spin-pumping current, assuming no voltage bias [18], is given by

$$\mathbf{I}_s(t) = \frac{1}{4\pi} g_{\text{eff}}^{\uparrow\downarrow} \mathbf{m} \times \partial_t \mathbf{m}, \quad (6)$$

where the effective mixing conductance is defined as fol-

lows:

$$g_{\text{eff}}^{\uparrow\downarrow} \equiv \int_{-\infty}^{\infty} d\varepsilon \partial_{\varepsilon} f(\varepsilon) \text{Re} g^{\uparrow\downarrow}. \quad (7)$$

Here, $f(\varepsilon) = (1 + e^{\varepsilon/k_B T})^{-1}$ is the Fermi-Dirac distribution and in order to properly take into account the temperature dependence of the S order, we have considered a temperature-dependent S gap $\Delta(T)$ [21].

In accordance with Eq. (6), the spin-pumping current in the direction of $\mathbf{m} \times \partial_t \mathbf{m}$ is simply determined by $g_{\text{eff}}^{\uparrow\downarrow}$, which can be regarded as the mixing conductance in the temperature domain. In order to focus on the role of ABS resonances, we have defined normalized effective conductance $\tilde{g}_{\text{eff}}^{\uparrow\downarrow} \equiv g_{\text{eff}}^{\uparrow\downarrow}(d_S)/g_{\text{eff}}^{\uparrow\downarrow}(d_S = 0)$. Here, $g_{\text{eff}}^{\uparrow\downarrow}(0)$ yields the effective conductance in the normal state. The resultant normalized conductance is plotted in Fig. 4. We find that, for subgap temperatures, $\tilde{g}_{\text{eff}}^{\uparrow\downarrow}$ shows a significant enhancement at the finite thickness of the S layer, i.e., $d_S \sim \xi_0$. The enhancement is optimal at the midgap temperatures and diminishes down to unity (the normal case) upon approaching T_c .

Before closing this paper, we explore the effect of a barrier potential at the S|N interface. Physically, this can originate from a thin oxide layer or a localized disorder on the interface. The essential effects of the interfacial scattering, caused by this layer, can be captured by a potential of the form $Z\hbar v_F \delta(x - d_S)$, where the dimensionless parameter Z determines strength of the barrier. Here, v_F is the Fermi velocity and $\delta(x)$ is the Dirac delta function.

At the S|N interface, a nonzero Z results in reduced transmission and AR probabilities by introducing ordinary electron and hole reflections [3]. This partially reflective interface can lead to the formation of normal bound states localized in the N layer. In contrast, the case of zero barrier ($Z = 0$) leads to ABSs only. For subgap energies, with the increase of Z the ordinary reflection probability surpasses the AR probability [3], which leads to ABSs to be pushed away from zero (towards the continuum of states above the gap) and replaced with ordinary bound states [15]. Consequently, in the strong barrier limit $Z > 1$, the subgap transport channels are due to the normal bound-state resonances, where superconductivity suppresses the spin pumping (see Fig. 5). We point out that the effective conductance is normalized with respect to $g_{\text{eff}}^{\uparrow\downarrow}(d_S = 0)$, which accounts for the contribution of the normal bound-state resonances. The weak barrier limit ($Z < 1$), on the other hand, can effectively be described within the zero-barrier limit by an increased d_N and Δ_{ex} (due to the multiple ordinary reflections) [see Fig. 5 (inset)].

Conclusion and discussion.—We have shown that superconductivity can greatly affect spin pumping due to the formation of the resonant ABSs, which result in highly transmitting spin transport channels when $d_S \sim$

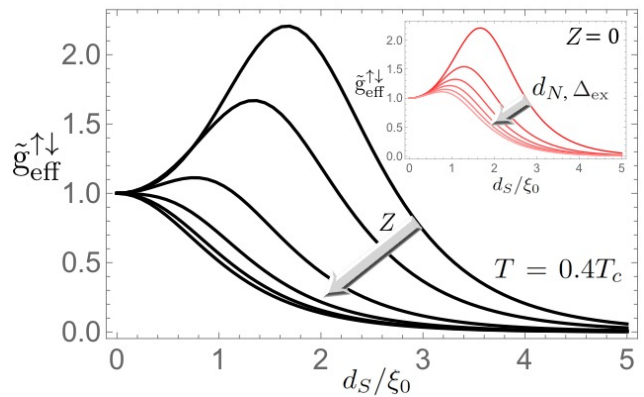


FIG. 5. The normalized effective conductance is shown for various barrier potential strengths Z , which are plotted by increasing Z in increments of 0.5 from 0 to 2.5. The enhancement feature ceases to exist for strong barriers $Z > 1$. The inset plot shows that the simultaneous increase of d_N and Δ_{ex} with $Z = 0$ can account for the conductance in the weak barrier case $Z < 1$. The red plots are generated by simultaneously increasing both the exchange interaction Δ_{ex}/E_F from 0.1 to 0.6 in increments of 0.1 and d_N/ξ_0 from 3 to 4.5 in increments of 0.3. In the above plots, we have set $d_N/\xi_0 = 3$, $\Delta_{\text{ex}}/E_F = 0.1$.

ξ_0 . This can be manifested experimentally by an increase in Gilbert damping of the FI dynamics. The Gilbert damping enhancement in an NbN|GdN structure has been observed to peak for subgap temperatures [5], where NbN is an s -wave superconductor with coherence length of ~ 5 nm that is adjacent to a ferromagnetic-insulator film, GdN. The enhancement takes place for $d_S = 10$ nm and it is suppressed for $d_S = 2$ nm. We believe that this is in good agreement with our results, e.g., Fig. 4. On the other hand, unfolding $N_r|S|N|FI$ effectively maps our setup to an $N_r|S|F|S|N_r$ structure, where F stands for a normal metal with a ferromagnetic order. The hybrid structure $N_r|Nb|Ni_{80}Fe_{20}|Nb|N_r$ studied in Ref. [4] shows a significant spin-pumping enhancement only when the Nb thickness is roughly equal to its coherence length ($d_S \approx \xi_0 = 30$ nm). In order to reveal a large enhancement, they have utilized a range of spin-sink materials N_r with spin-orbit interaction, such as Pt, W, or Ta. In Ref. [17] the same hybrid structure of Ref. [4] has been used except for a particularly magnetized spin sink Pt/Co/Pt. It is shown that the spin-pumping efficiency across Nb is tunable by controlling the magnetization direction of Co.

Furthermore, hybrid Josephson junctions realizing ABSs with near unity transmission probability for charge transport have been proposed to coherently manipulate quantum-information devices such as Andreev-level qubits [29, 30]. From this standpoint, unfolding our setup realizes a magnetically active Josephson junction [8] with resonant transport channels, which in turn can provide a spintronic paradigm for a coherent manipulation of quan-

tum–information devices involving ABSs. *Note added:* Recently, we became aware of an interesting and closely related work by Silaev [31].

It is a pleasure to acknowledge discussions with C. Ciccarelli and W. A. Robinson who drew our attention to this problem. MTA wishes to thank S. Tanhayi Ahari for useful comments on the paper. This work is supported by the U.S. Department of Energy, Office of Basic Energy Sciences under Grant No. DE-SC0012190.

-
- [1] J.-D. Pillet, C. H. L. Quay, P. Morfin, C. Bena, A. Levy Yeyati, and P. Joyez, *Nat. Phys.* **6**, 965 (2010); J. Schindele, A. Baumgartner, R. Maurand, M. Weiss, and C. Schönenberger, *Phys. Rev. B* **89**, 045422 (2014); J. A. Sauls, *Phil. Trans. R. Soc. A* 37620180140 (2018)
- [2] E. J. H. Lee, X. Jiang, M. Houzet, R. Aguado, C. M. Lieber, and S. De Franceschi, *Nature Nanotechnology*, **9**, 79 (2014); F. Pawlicki and I. Weymann, *Phys. Rev. B* **98**, 085411 (2018)
- [3] Y. Tserkovnyak, A. Brataas, G. E. W. Bauer, and Bertrand I. Halperin, *Rev. Mod. Phys.* **77**, 1375 (2005)
- [4] K-R Jeon, C. Ciccarelli, A. J. Ferguson, H. Kurebayashi, L. F. Cohen, X. Montiel, M. Eschrig, J. W. A. Robinson, and M. G. Blamire, *Nat. Mater.* **17**, 499–503 (2018)
- [5] Y. Yao, Q. Song, Y. Takamura, and et al, *Phys. Rev. B* **97**, 224414 (2018)
- [6] S. Kashiwaya, Y. Tanaka, N. Yoshida, and M. R. Beasley, *Phys. Rev. B* **60**, 3572 (1999)
- [7] J. Linder, J. W. A. Robinson, *Nature Physics*, **11**, 307–315 (2015)
- [8] M. Fogelström, *Phys. Rev. B* **62**, 11812, (2000)
- [9] M. Eschrig, J. Kopu, J. C. Cuevas, G. Schön, *Phys. Rev. Lett.* **90**, 137003 (2003); G. Metalidis, M. Eschrig, R. Grein, G. Schön, *Phys. Rev. B* **82**, 180503(R) (2010); H. Yang, S-H Yang, S. Takahashi, S. Maekawa, and S. S. P. Parkin, *Nat. Mater.* **9**, 586 (2010)
- [10] A. Brataas and Y. Tserkovnyak, *Phys. Rev. Lett.* **93**, 087201 (2004)
- [11] F. S. Bergeret, A. F. Volkov, and K. B. Efetov, *Phys. Rev. Lett.* **86**, 4096 (2001)
M. Houzet and A. I. Buzdin, *Phys. Rev. B* **76**, 060504(R) (2007)
- [12] M. Eschrig, *Phil. Trans. R. Soc. A* 376: 20150149 (2018)
- [13] T. Vezin, C. Shen, J. E. Han, and I. Žutić, *Phys. Rev. B* **101**, 014515 (2020)
- [14] T. Yokoyama, and Y. Tserkovnyak, *Phys. Rev. B* **80**, 035408 (2009)
- [15] See the Supplemental Material at <https://link.aps.org/supplemental/DOI> for a discussion of multichannel scattering, exact expressions of the reflection amplitudes, and a heuristic argument for the dynamic generation of triplet pairing. We also provide a brief discussion of the ABS modification in the presence of the interface barrier potential.
- [16] M. Inoue, M. Ichioka, and H. Adachi, *Phys. Rev. B* **96**, 024414 (2017)
- [17] K-R Jeon, X. Montiel, S. Komori, C. Ciccarelli, J. Haigh, H. Kurebayashi, L. F. Cohen, A. K. Chan, K. D. Stenning, C-M Lee, M. G. Blamire, and J. W. A. Robinson, *Phys. Rev. X* **10**, 031020 (2020)
- [18] H. J. Skadsem, A. Brataas, J. Martinek, and Y. Tserkovnyak, *Phys. Rev. B* **84**, 104420 (2011)
- [19] B. Belchev, S.G. Neale, M.A. Walton, *Can. J. Phys.* **89**, 11 (2011)
- [20] Y. Nazarov, Y. Blanter. *Quantum Transport: Introduction to Nanoscience*. Cambridge: Cambridge University Press (2009)
- [21] We consider an energy gap of $1.1E_F$ for up-spin and $1.1E_F + 2\Delta_{ex}$ for down-spin electrons. The Fermi energy E_F is assumed to be identical for the different layers, $E_F = 5$ eV. Furthermore, we have assumed Nb as the S with $T_c = 9$ K, $\xi_0 = 30$ nm, and $\Delta_0 = 3$ meV. We have adopted the following empirical parametrization for a temperature-dependent superconductor gap for Nb, $\Delta(T) = \Delta_0(1 - T/T_c)^{1.94}(1 + 2.17T/T_c)$, that is taken from R. C. Dougherty, J. D. Kimel. *Superconductivity Revisited*. (CRC Press, Boca Raton, FL, 2012)
- [22] A. Brataas, Y. V. Nazarov, and G. E. W. Bauer, *Phys. Rev. Lett.* **84**, 2481 (2000)
- [23] F. Hübner, M. J. Wolf, T. Scherer, D. Wang, D. Beckmann, and H. v. Löhneysen, *Phys. Rev. Lett.* **109**, 087004 (2012)
- [24] H. van Houten, C. W. J. Beenakker, *Physica B: Condensed Matter* **175**, Issues 1–3, (1991)
- [25] N. Ismail, C. C. Kores, D. Geskus, and M. Pollnau, *Optics Express* Vol. 24, Issue 15, (2016)
- [26] W. J. Tomasch, *Phys. Rev. Lett.* **16**, 16 (1966).
- [27] K. Xia, P. J. Kelly, G. E. W. Bauer, and I. Turek, *Phys. Rev. Lett.* **89**, 166603 (2002)
- [28] G. E. Blonder, M. Tinkham, and T. M. Klapwijk. *Phys. Rev. B* **25**, 4515 (1982)
- [29] F. Nichele, E. Portoles, A. Fornieri, A. M. Whiticar, A. C. C. Drachmann, S. Gronin, T. Wang, G. C. Gardner, C. Thomas, A. T. Hatke, M. J. Manfra, and C. M. Marcus, *Phys. Rev. Lett.* **124**, 226801 (2020)
- [30] J. Michelsen, V. S. Shumeiko, and G. Wendin *Phys. Rev. B* **77**, 184506 (2008); C. Janvier, L. Tosi, L. Bretheau, C. Ö. Girit, M. Stern, P. Bertet, P. Joyez, D. Vion, D. Esteve, M. F. Goffman, H. Pothier, C. Urbina, *Science* **349**, Issue 6253, (2015)
- [31] M. A. Silaev, *Phys. Rev. B* **102**, 180502(R) (2020)

Supplementary Material for Superconductivity-enhanced spin pumping: Role of Andreev resonances

Mostafa Tanhayi Ahari, Yaroslav Tserkovnyak

Department of Physics and Astronomy, University of California, Los Angeles, California 90095, USA

In this supplementary material, we discuss a QP scattering formalism that takes into account the dynamic magnetization of the FI and the s -wave order of the S in an $N_r|S|N|FI$ hybrid structure, see Fig. S1. We will derive analytical expressions for the scattering amplitudes, ABS modification under an interfacial disorder, and elaborate on the dynamic generation of the triplet Cooper pairs in our setup.

Spin-dependent scattering.—In the context of QP scattering in hybrid structures generic boundary conditions pertinent to interface scattering and disorder can be taken into account by insertion of a perfect spacer N between adjacent materials [1, 2]. As such, the full scattering process can be broken down into studying $N_r|S|N$, and $N|FI$ structures separately. We bear in mind that propagation through the N layer mixes neither particle-hole nor spin degrees of freedom. For the $N_r|S|N$ structure, following BTK [3], we assume a uniform superconducting pair-potential Δ inside the S layer that vanishes in the N layer. This way the scattering process takes place only at the interfaces, which essentially contains QPs propagating into the S and Andreev retroreflection. In a more realistic (dirty) N|S interface, however, there is a possibility of a specular reflection for electrons and holes. In order to model the partially reflective interface, we can consider a barrier potential in the form of $V = Z_1 \hbar v_F \delta(x)$ and $Z_2 \hbar v_F \delta(x - d_S)$. A finite Z_1 , leads to quantum interference with the Fermi wavelength and does not affect ABS. In the following, we set $Z_1 = 0$ and focus on the effect of a nonzero $Z_2 \equiv Z$.

Initially, we study point contact scattering in a 1D wire. Physically, this can be justified by imposing a constriction, for which the transverse thickness of the N layer is on the order of the Fermi wavelength [1]. Later on, we will relax this condition by considering a 3D geometry for which the incident QPs can have a transverse momentum.

We begin with the BdG formalism that accounts for symmetries of the superconducting part for the electron and hole wave functions,

$$H_{\text{BdG}}\Psi = \varepsilon\Psi, \quad \text{with} \quad H_{\text{BdG}} = \begin{pmatrix} \hat{H}_0 & \hat{\Delta} \\ \hat{\Delta}^\dagger & -\hat{H}_0^* \end{pmatrix}, \quad (\text{S1})$$

where $\hat{H}_0 = (\mathbf{p}^2/2m + V - E_F)$ is the single-electron Hamiltonian matrix and $\hat{\Delta} = \Delta i\sigma_y$. Here, we assume a real-valued pairing potential Δ . The Pauli matrix σ_y is acting on the spin space $\{\uparrow, \downarrow\}$ of conduction electrons and holes. Above eigenvalue equation admits the following basic electron and hole QP modes with spin σ :

$$\begin{aligned} \Psi_{n,e\sigma}^\pm &= \begin{pmatrix} \chi_\sigma \\ A(\varepsilon)(-i\sigma_y)\chi_\sigma \end{pmatrix} e^{\pm iq_e x} e^{i\mathbf{k}_\parallel \cdot \mathbf{r}_\parallel}, \\ \Psi_{n,h\sigma}^\pm &= \begin{pmatrix} A^*(-\varepsilon)(-i\sigma_y)\chi_\sigma \\ \chi_\sigma \end{pmatrix} e^{\pm iq_h x} e^{i\mathbf{k}_\parallel \cdot \mathbf{r}_\parallel}, \end{aligned} \quad (\text{S2})$$

where $\chi_\uparrow = \begin{pmatrix} 1 \\ 0 \end{pmatrix}$, $\chi_\downarrow = (-i\sigma_y)\chi_\uparrow$, are two dimensional spinors, and we have

$$\frac{\hbar^2}{2m} q_{e,h}^2 = E_F - E_n + \zeta^{e,h} \Omega, \quad \Omega \equiv \begin{cases} i\sqrt{\Delta^2 - \varepsilon^2}, & \text{if } |\varepsilon| < \Delta \\ \varepsilon\sqrt{1 - \Delta^2/\varepsilon^2}, & \text{if } |\varepsilon| > \Delta \end{cases}, \quad A(\varepsilon) = \begin{cases} e^{-i \arccos(\varepsilon/\Delta)}, & |\varepsilon| < \Delta \\ \frac{\varepsilon - \varepsilon\sqrt{1 - \Delta^2/\varepsilon^2}}{\Delta}, & |\varepsilon| > \Delta \end{cases}, \quad (\text{S3})$$

where $E_n \equiv \hbar^2 k_\parallel^2/2m$, and $\zeta^{e,h} = \pm 1$. In the normal layer, the wave number is given by $k_{e,h} = q_{e,h}(\Delta \rightarrow 0)$. The conservation of the QP spin leads to a block diagonal full scattering matrix in the spin space. Whence, we can work with the following 2 dimensional eigen vectors,

$$\begin{aligned} \Psi_{Sne}^\pm &= \begin{pmatrix} 1 \\ A(\varepsilon) \end{pmatrix} e^{\pm iq_e x} e^{i\mathbf{k}_\parallel \cdot \mathbf{r}_\parallel}, \\ \Psi_{Snh}^\pm &= \begin{pmatrix} A(\varepsilon) \\ 1 \end{pmatrix} e^{\pm iq_h x} e^{i\mathbf{k}_\parallel \cdot \mathbf{r}_\parallel}. \end{aligned} \quad (\text{S4})$$

It is clear that outside of the S, where $\Delta \rightarrow 0$, we get $A(\varepsilon) \rightarrow 0$, leading to normal region's basis elements,

$$\begin{aligned} \Psi_{Nne}^\pm &= \begin{pmatrix} 1 \\ 0 \end{pmatrix} e^{\pm ik_e x} \Phi_n(y, z), \\ \Psi_{Nnh}^\pm &= \begin{pmatrix} 0 \\ 1 \end{pmatrix} e^{\pm ik_h x} \Phi_n(y, z), \end{aligned} \quad (\text{S5})$$

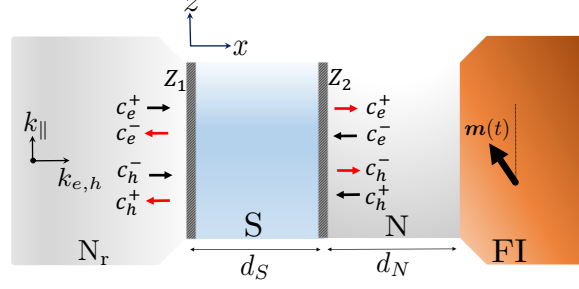


FIG. S1. A snapshot configuration for the magnetization $\mathbf{m}(t)$ in an $N_r|S|N|FI$ structure with the incoming and outgoing modes into the S (black and red, respectively). The propagation direction for electrons and holes with scattering amplitudes c_e^\pm, c_h^\pm are given by $\pm\hat{\mathbf{x}}, \mp\hat{\mathbf{x}}$, respectively. The shaded slabs at $x = 0$ and d_S represent the barrier potentials whose strengths are parametrized by Z_1 and Z_2 . The incident QP wave vector is given by $(k_{e,h}, k_{\parallel})$.

Therefore, the incident and reflected modes in N and S layers can be expanded as

$$\Psi_N = c_e^+(N)\Psi_{Nne}^+ + c_e^-(N)\Psi_{Nne}^- + c_h^+(N)\Psi_{Nnh}^+ + c_h^-(N)\Psi_{Nnh}^-, \quad (\text{S6})$$

and

$$\Psi_S = c_e^+(S)\Psi_{Sne}^+ + c_e^-(S)\Psi_{Sne}^- + c_h^+(S)\Psi_{Snh}^+ + c_h^-(S)\Psi_{Snh}^-. \quad (\text{S7})$$

The scattering matrix across the S is obtained by imposing the following conditions: (1) continuity of the wave functions and their derivative at the interfaces $x = 0, d_S$, (2) continuity of the current inside the S, that is, $0 < x < d_S$. A straight forward algebra, under Andreev approximation $\Delta/E_F \ll 1$, yields

$$\begin{pmatrix} c_e^-(N_r) \\ c_e^+(N) \\ c_h^+(N_r) \\ c_h^-(N) \end{pmatrix} = \frac{1}{1 - A^2\gamma} \begin{pmatrix} 0 & \kappa\gamma u^{-2} & A(1 - \gamma) & 0 \\ \kappa\gamma u^{-2} & 0 & 0 & A(1 - \gamma) \\ A(1 - \gamma) & 0 & 0 & \gamma\kappa^{-1}u^{-2} \\ 0 & A(1 - \gamma) & \gamma\kappa^{-1}u^{-2} & 0 \end{pmatrix} \begin{pmatrix} c_e^+(N_r) \\ c_e^-(N) \\ c_h^-(N_r) \\ c_h^+(N) \end{pmatrix}, \quad (\text{S8})$$

where

$$\begin{aligned} \kappa &= e^{ik_F d_S}, \quad \gamma = e^{i2\Omega d_S/\hbar v_F}, \\ u^2 &= \frac{\varepsilon}{\Omega} \left(\frac{1}{2} + \frac{\Omega}{2\varepsilon} \right), \quad r_A^\infty \equiv A. \end{aligned} \quad (\text{S9})$$

The quantity r_A^∞ is the AR amplitude at the interface of a normal metal with a bulk S [1]. For a thin S layer, as it can be checked from the QP scattering matrix for the $N_r|S|N$ structure, this is modified to

$$r_A = \frac{(1 - \gamma)(r_A^\infty)}{1 - \gamma(r_A^\infty)^2}. \quad (\text{S10})$$

The scattering matrix can be generalized [4] to include a nonzero barrier potential at the interface $x = d_S$. We note that, within the Andreev approximation $\Delta/E_F \ll 1$, the transmission amplitude for electrons is given by $1/(1 + iZ)$. We study the case of nonzero barrier numerically. The electrons and holes propagate through the normal metal and reflect back off the FI interface,

$$\begin{aligned} c_e^-(N) &= r_e^\sigma c_e^+(N), \\ c_h^+(N) &= r_h^{-\sigma} c_h^-(N), \end{aligned} \quad (\text{S11})$$

where the electron reflection coefficient is given by $r_e^\sigma(\varepsilon) \approx e^{i(k_F + \varepsilon/\hbar v_F)2d_N} e^{i\vartheta_\sigma}$, and particle-hole symmetry yields $r_h^\sigma(\varepsilon) = [r_e^\sigma(-\varepsilon)]^*$. The spin-dependent phase shift ϑ_σ is given by

$$e^{i\vartheta_\sigma} = \frac{\sqrt{E} - i\sqrt{V_\sigma - E}}{\sqrt{E} + i\sqrt{V_\sigma - E}}, \quad E < V_\sigma. \quad (\text{S12})$$

The energy of an incoming electron or hole is given by $E = \hbar^2 k_{e,h}^2/2m$. Combining the scattering matrix of $N_r|S|N$ with Eq. (S11), the full scattering matrix with single channel obtains ($Z = 0$),

$$\begin{pmatrix} c_e^-(N_r) \\ c_h^+(N_r) \end{pmatrix} = \begin{pmatrix} r_{ee}^\sigma & r_{eh}^{-\sigma} \\ r_{he}^\sigma & r_{hh}^{-\sigma} \end{pmatrix} \begin{pmatrix} c_e^+(N_r) \\ c_h^-(N_r) \end{pmatrix}, \quad (\text{S13})$$

where

$$\begin{aligned} r_{ee}^\sigma &= \frac{\kappa^2 \gamma}{\eta} r_e^\sigma, & r_{hh}^{-\sigma} &= \frac{\kappa^{-2} \gamma}{\eta} r_h^{-\sigma}, \\ r_{he}^\sigma &= r_{eh}^{-\sigma} = \frac{r_A^\infty (1 - \gamma)}{\eta} \left[1 - (r_A^\infty)^2 \gamma - ((r_A^\infty)^2 - \gamma) r_e^\sigma r_h^{-\sigma} \right]. \end{aligned}$$

In the above equations we have defined

$$\eta \equiv (1 - (r_A^\infty)^2 \gamma)^2 - (r_A^\infty)^2 (1 - \gamma)^2 r_e^\sigma r_h^{-\sigma}. \quad (\text{S14})$$

It is instructive to note that a constructive Rowell–McMillan interference takes place when

$$r_e^\sigma r_h^{-\sigma} (r_A^\infty)^2 = e^{i2n\pi}, \quad n = 0, \pm 1, \pm 2, \dots, \quad (\text{S15})$$

The extra terms in η stem from multiple tunneling and AR reflection possibilities due to finite thickness of the S ($\gamma \neq 0$). In short, the scattering matrix with all the nonzero elements can be written as follows:

$$S(\varepsilon) = \begin{pmatrix} r_{ee}^\uparrow(\varepsilon) & 0 & 0 & r_{eh}^\downarrow(\varepsilon) \\ 0 & r_{ee}^\downarrow(\varepsilon) & r_{eh}^\uparrow(\varepsilon) & 0 \\ 0 & r_{he}^\downarrow(\varepsilon) & r_{hh}^\uparrow(\varepsilon) & 0 \\ r_{he}^\uparrow(\varepsilon) & 0 & 0 & r_{hh}^\downarrow(\varepsilon) \end{pmatrix}. \quad (\text{S16})$$

Time-dependent scattering.—A comparison between a typical FI precession period $\sim 10^{-10}$ s (FMR period) with the time scales of electron and hole dynamics, $(d_S + d_N)/v_F \ll 10^{-10}$ s, reveals that the magnetization dynamics can be taken as an adiabatic evolution during the scattering process. Initially, this reduces the problem to a time-independent process carried out with a snapshot configuration for the magnetization. Nonetheless, one can generalize to incorporate magnetization precession dynamics with a simple time-dependent $SU(2)$ rotation to the lab frame in which the magnetization direction is varying [5]. Including the precessional motion of the magnetization, $\mathbf{m}(t) = (\sin \theta \cos \omega t, \sin \theta \sin \omega t, \cos \theta)$, can be accomplished by a spinor rotation [5] given by

$$U(t) = \begin{pmatrix} e^{i\frac{\theta}{2}\sigma_y} & 0 \\ 0 & e^{i\frac{\theta}{2}\sigma_y} \end{pmatrix} \begin{pmatrix} e^{i\frac{\omega t}{2}\sigma_z} & 0 \\ 0 & e^{-i\frac{\omega t}{2}\sigma_z} \end{pmatrix}, \quad (\text{S17})$$

where ω is the precessional angular speed. Consequently, the time dependent scattering matrix in the lab frame obtains, $S(\varepsilon, t) = U^\dagger(t) S(\varepsilon) U(t)$.

Andreev resonances.—The condition given in Eq. (S15) corresponds to the resonant behavior in the mixing conductance, which determines Andreev bound-state excitation energies ε_A . It can be checked that, the low energy ABSs can only form when $d_N > 0$. This indicates that, in the limit of zero barrier, the insertion of a normal metal layer not only provides a level of control but is a necessary element for the enhancement of spin flow. By increasing the barrier potential strength, however, subgap normal bound states begin to form and ABSs are pushed away from the subgap region (see Fig. S2). In order to see this, we have defined

$$f_{\text{ABS}}(Z) \equiv \text{Re } g^{\uparrow\downarrow}(d_S, d_N, \varepsilon_{\text{res}}, Z) - \text{Re } g^{\uparrow\downarrow}(d_S, d_N, \varepsilon_{\text{res}}, Z_\infty). \quad (\text{S18})$$

Here, ε_{res} represent resonance energies, for which the real part of the conductance is maximum. Note that, $\varepsilon_{\text{res}} \rightarrow \varepsilon_A$ when $Z \rightarrow 0$. Since $Z_\infty \gg 1$, $\text{Re } g^{\uparrow\downarrow}(d_S, d_N, \varepsilon_{\text{res}}, Z_\infty)$ includes only normal bound-state resonances.

3D geometry.—Due to the translation symmetry on the interfaces, the full 3D scattering problem can be inferred from our scattering matrix given in Eq. (S16). As we have mentioned earlier, the wave number for the electron and hole propagating at energy ε is given by

$$k_{e,h}^n = \sqrt{\frac{2m}{\hbar^2}} \sqrt{E_F - E_n + \zeta^{e,h} \varepsilon}, \quad (\text{S19})$$

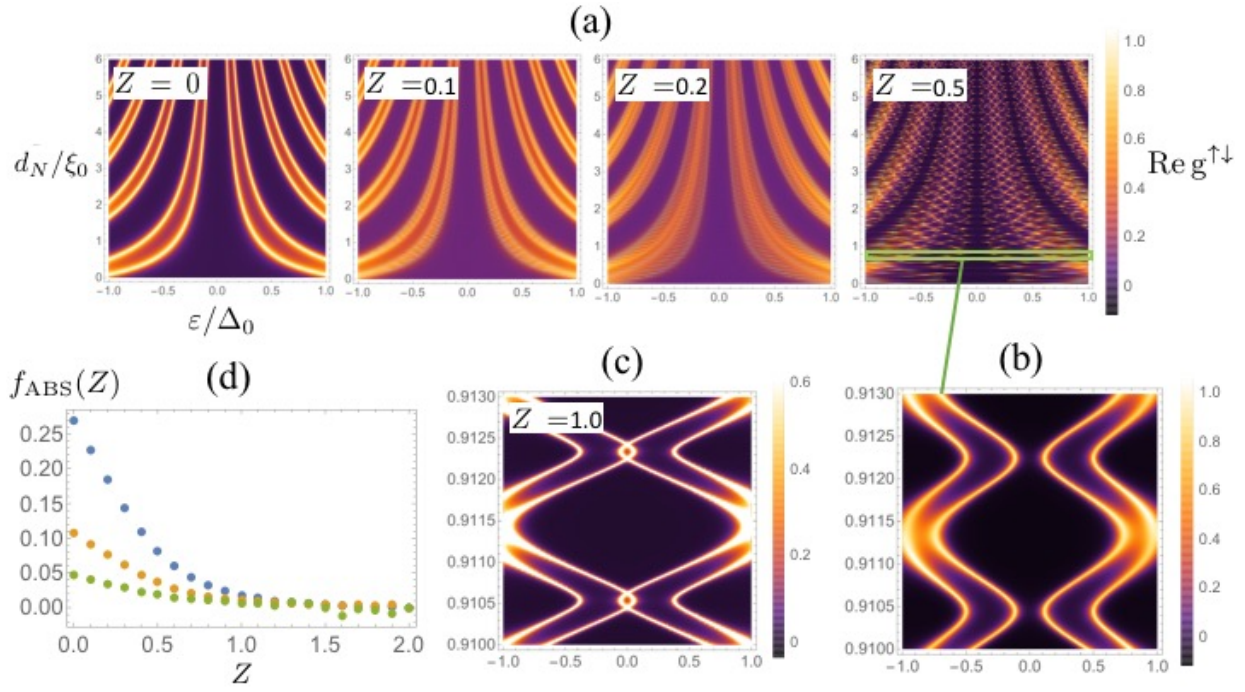


FIG. S2. (a) The resonant bound-state energies, ε_{res} , for various Z . When $Z = 0$, we get $\varepsilon_{\text{res}} = \varepsilon_A$. (b) For finite but small barrier strength, $\text{Re } g^{\uparrow\downarrow}$ has contribution from normal and Andreev bound-state resonances. (c) For the stronger barrier, when the AR probability is negligible, the resonant energies are due to normal bound states. In (a), (b), and (c), we have set $d_S/\xi_0 = 1.5$ and $\Delta_{\text{ex}} = 0.4E_F$. (d) $f_{\text{ABS}}(Z)$ is shown for $Z_\infty = 2$, where the blue, orange, and green curves correspond to $d_S/\xi_0 = 1, 1.5$, and 2 , respectively. In this plot, we have $\Delta_{\text{ex}} = 0.4E_F$ and $d_N/\xi_0 = 1$.

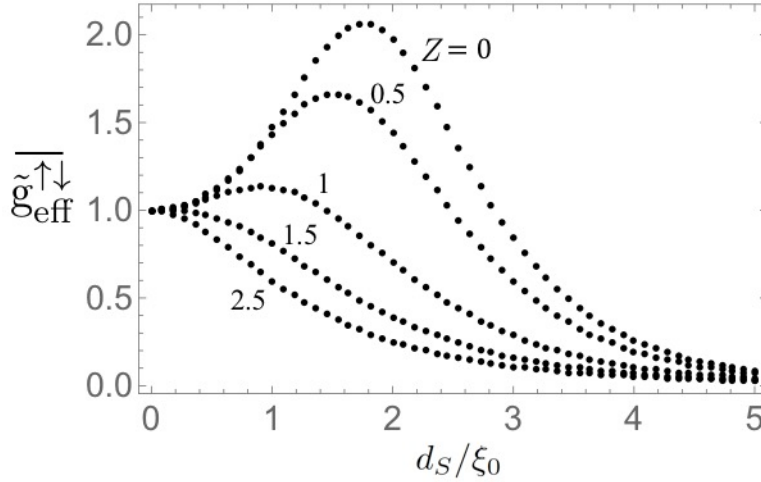


FIG. S3. The normalized conductance averaged over $N(\varepsilon) = 20$ channels in ballistic regime for various barrier strengths Z . Here, we have set $\Delta_{\text{ex}}/E_F = 0.1$, $T/T_c = 0.4$, and $d_N/\xi_0 = 2.5$.

where E_n is the transverse energy of the incident electron or hole. Here, the channel number index n is considered to distinguish QPs propagating through different channels at energy ε . The multichannel effective conductance is obtained by summing over all the channels present at energy ε . We consider $N(\varepsilon)$ to denote the total number of such channels. In Fig. S3, we have shown normalized effective conductance for multichannel case in the presence of interface barrier potential.

Dynamic generation of triplet Cooper pairs—We utilize a heuristic argument to describe the triplet pairing generation in our setup. For a thin S layer, $d_S \sim \xi_0$, QPs with the resonant energies can escape the N layer either by

tunnelling through the S layer or forming Cooper pairs inside the S layer. For the latter case, the Cooper pairs contain the spin-dependent phases as follows [6]:

$$e^{i\alpha} |\uparrow\downarrow\rangle - e^{-i\alpha} |\downarrow\uparrow\rangle, \quad (\text{S20})$$

where $\alpha \sim \vartheta$. These Cooper pairs contain a spin-triplet component, $|\uparrow\downarrow\rangle + |\downarrow\uparrow\rangle$, with an amplitude determined by $\sin \alpha$. The precessing magnetization \mathbf{m} can dynamically induce spin-polarized triplet Cooper pairs $|\downarrow\downarrow\rangle$ and $|\uparrow\uparrow\rangle$, which is caused by the variations in the direction of the quantization axis for spins [6]. In other words, the spin-polarized triplet components arise when the spin-triplet component $|\uparrow\downarrow\rangle + |\downarrow\uparrow\rangle$ is written in a new rotated basis [6].

-
- [1] C. W. J. Beenakker. Rev. Mod. Phys. **69**, 731 (1997)
 - [2] Y. Nazarov, Y. Blanter. Quantum Transport: Introduction to Nanoscience. Cambridge: Cambridge University Press (2009)
 - [3] G. E. Blonder, M. Tinkham, and T. M. Klapwijk. Phys. Rev. B **25**, 4515 (1982)
 - [4] O. Entin-Wohlman, Y. Imry, and A. Aharony. Phys. Rev. B **78**, 224510 (2008)
 - [5] H. J. Skadsem, A. Brataas, J. Martinek, and Y. Tserkovnyak, Phys. Rev. B **84**, 104420 (2011)
 - [6] M. Eschrig, T. Löfwander. Nature Physics, **4**, (2008)
J. Linder, J. W. A. Robinson, Nature Physics, **11**, (2015)